ELSEVIER

Polymer 42 (2001) 5293–5306

polymer

www.elsevier.nl/locate/polymer

The effect of cyclic true strain on the morphology, structure, and relaxation behavior of ultra high molecular weight polyethylene

R.W. Meyer, L.A. Pruitt*

Department of Mechanical Engineering, University of California, 5134 Etchevery Hall, 1740, Berkeley, CA 94720-1740, USA

Received 29 June 2000; received in revised form 7 August 2000; accepted 14 August 2000

Abstract

Cyclic loading of total joint replacement bearing materials made of ultra high molecular weight polyethylene (UHMWPE) can lead to fatigue failures and the generation of wear particles resulting from the accumulation of plastic strain. Susceptibility to damage processes can be further complicated by choice of sterilization method and shelf aging prior to implantation. The objective of this study was to characterize the effects of cyclic true tensile strain on the morphological evolution and mechanical relaxation behavior of both non-sterile and radiation sterilized medical grade UHMWPE. A γ-radiation sterilization process with several years of shelf aging was utilized in order to discern morphological changes and mechanical behavior resulting from oxidative degradation coupled with cyclic loading. A video-based true stress–strain measurement system was developed and validated to characterize the true stress–strain behavior of the UHMWPE. Non-sterile and sterilized specimens were each subjected to a range of true strain over a number of loading cycles. Following each test, strain recovery data was collected and final residual plastic strain was determined. Density gradient column measurements were conducted to provide evidence of structural changes that resulted from the cyclic strain tests. Scanning electron and field emission microscopy were utilized to provide further evidence of the morphological evolution of the UHMWPE. This study showed that the morphological evolution of both the non-sterile and sterile material groups could be correlated with the amount of true strain and the number of cycles. Furthermore, these differences in the behavior of the two materials could be attributed to their distinct initial microstructure. The results of this study have important implications for the development of constitutive and phenomenological models that may incorporate morphological evolution in UHMWPE and other semi-crystalline polymers.

Keywords: UHMWPE; Cyclic true strain; Morphology

1. Introduction

Ultra high molecular weight polyethylene (UHMWPE) has been utilized as the synthetic replacement for articular cartilage in total joint replacements for nearly four decades [1]. The choice of this polymer as a bearing material stems from its superior biomechanical properties including high toughness, low friction coefficient and good biocompatibility. However, despite its attributes and widespread use, it remains the limiting component in the life of these prosthetic devices. This limitation arises because of the generation of mechanically induced polymer debris at the articulating surface. Although the precise wear mechanisms are not fully understood, recent studies suggest that submicron wear particles are the result of an accumulated amount of critical plastic strain in the UHMWPE component [2,3]. Furthermore, this cyclic loading can propagate surface and subsurface fatigue cracks, which can result in local fracture, delamination, and pitting of the polyethylene [4–7]. Another complicating factor in total joint replacements is the choice of sterilization method for the polyethylene components. This sterilization process can affect the material behavior of the polymer and previous work has shown the detrimental effects of morphological evolution on the modulus and strain hardening behavior of UHMWPE associated with ionizing radiation sterilization methods [8–10]. This study investigates the combined effects of cyclic strain and sterilization on the mechanical behavior and morphological development of UHMWPE.

The evolution of microstructural features within the polyethylene as a result of accumulated plastic strain are believed to be key in understanding the mechanisms of fracture and wear processes in tough polymers. At the microstructural level, UHMWPE comprises crystalline lamellae embedded in an amorphous matrix. Due to the very high molecular weight of UHMWPE there is a tendency for a high degree of chain entanglement in the

* Corresponding author. Tel.: +1-510-642-2595; fax: +1-510-643-5599.
E-mail address: lpruitt@newton.berkeley.ed (L.A. Pruitt).

0032-3861/01/$ - see front matter
PII: S0032-3861(00)00626-1

amorphous phase and molecular interconnects between lamellae known as 'tie molecules'. These tie molecules help to provide additional resistance to mechanical deformation and give rise to the exceptional toughness observed in UHMWPE [11,12]. The initial morphology of UHMWPE can vary widely depending on the starting resin, the manufacturing process utilized to generate the material, and the sterilization process utilized to prepare the joint components for implantation within the body [7].

Sterilization of the orthopedic components is required prior to implantation. γ-radiation, typically with a dose between 25 and 40 kGy from a ^{60}Co source, in an inert environment is a common sterilization technique utilized by the medical industry. Ionizing radiation, however, results in the generation of free radicals, which then lead to a competition between cross-linking and scission depending on the chemical environment [13,14]. In general, cross-linking is favored when ionizing radiation is performed in an inert environment while scission dominates if radiation is performed in the presence of oxygen. The free radicals generated in the crystalline regions of the polymer have long lifetimes and can slowly diffuse to the crystalline–amorphous boundary, where the radicals undergo chemical reactions with oxygen that has diffused from the environment [15–18]. The scission of tie molecules associated with these oxidative degradation results in a structure with higher crystallinity and density due to more efficient packing of the shorter chains. Recent studies by Kurtz et al. [10] have shown lamellae reorganization and enhanced packing in UHMWPE that has been subjected to γ-radiation and aged through accelerated methods. Accompanying oxidative degradation and processing factors, plastic deformation also affects the degree of texturing and other morphological characteristics.

In a clinical realm, there is strong evidence that preferential orientation of lamellae or texturing results in degraded tribological properties and wear performance of UHMWPE devices [19]. In fact, plasticity-based degradation of polyethylene is an important problem for industry and has been the subject of numerous research studies [20–31]. Peterlin [20] describes the morphological evolution of polyethylene subjected to tensile loading that results in texturing and the development of a new long period in the crystalline portion of the polymer. Galeski et al. [21] use similar arguments to describe this texturing process for polyethylene subjected to compression in a channel die. Lin and Argon describe extensively the mechanisms of plastic flow in high density polyethylene at high levels of strain [22]. More recently, Kurtz et al. [2] and G'Sell et al. [23] have studied such phenomenon in UHMWPE at high plastic strain for both uniaxial and biaxial loading conditions as well as for clinical devices. In addition, recent work by Wimmer [24] has investigated the morphological evolution in the knee joint.

The details of morphological evolution depend on the initial microstructure, loading conditions and test environment, nonetheless it is believed that the plastic flow of polyethylene initiates in the amorphous phase before transitioning into the crystalline phase of the polymer. Deformation in the amorphous phase is believed to occur through chain slip [25,26] interlamellar shear [27], interlamellar separation [28], and lamella-stack rotation [29,30]. In highly crystalline polymers above the glass transition temperature, the deformation of the amorphous component is rapidly exhausted and further deformation occurs primarily in the crystalline lamellae. The lamellae plasticity is postulated to occur predominantly through crystallographic slip [31] but also can occur through mechanical twinning and stress-induced martensitic transformations [32,33]. In UHMWPE, because of the large predominance of tie molecules, there also may be lamellae-based plasticity in the crystalline phases at much lower strains [21,23,34]. In addition, interlamellar separation, present during tensile deformation, can result in stress whitening and cavitation or microvoid formation within the polymer [23,35–37]. In order to develop microstructurally based constitutive equations for UHMWPE, it is imperative that microstructural changes be correlated with true stresses and strains in the material.

Extensive research over the past two decades on semi-crystalline polymers has shown the importance of true stress–strain curves in providing useful information about the yielding behavior, the true rate of strain hardening, and the stress-induced transformations of crystalline phases within the polymer [2,23,37]. Furthermore, true stress–strain behavior can be used in the development of constitutive relationships and finite element models to accurately predict multiaxial stress states in complex geometries, such as those employed in the acetabular and tibial components of total joint replacements. This study characterizes the true stress–strain behavior of UHMWPE and examines the structural evolution due to the combined effects of ionizing radiation, shelf aging and cyclic loading. Both non-sterile and irradiated specimens of UHMWPE are subjected to varying cyclic tensile strains and analyzed using a novel, video true stress–strain measurement apparatus. Residual plasticity and density of the specimens are measured following cyclic loading of the UHMWPE. Scanning electron microscopy (SEM) and field emission microscopy (FEM) are utilized to study micromechanisms of deformation and to correlate the effect of cyclic true strain on the UHMWPE morphology.

2. Experimental methods

2.1. Materials

The material used for this study was ram extruded GUR 4150 (Hoechst Celanese) medical grade UHMWPE. The material properties are listed in Table 1. Tensile specimens were machined from the extruded UHMWPE into dog bones per ASTM standard D638-97 type III with the

Table 1
Physical properties of UHMWPE

Property	GUR 1150
Molecular weight	3–6 million g/mol
Crystallinity	45–50%
Density	0.93–0.935
Ultimate tensile strength (21°C)	42–44 MPa
Ultimate tensile strength (37°C)	36 MPa
Yield strength (21°C)	20–23 MPa
Yield strength (37°C)	21 MPa
Elastic modulus (21°C)	1.0–1.39 GPa
Elastic modulus (37°C)	0.67 GPa
Elongation at break (21°C)	330%
Elongation at break (37°C)	375%
Shore D hardness (21°C)	60–65

following geometry: gage width, $W = 19$ mm; length of narrow section, $L = 57$ mm; grip width, WO = 29 mm; overall length, LO = 246 mm; gage length, $G = 50$ mm; distance between grips, $D = 115$ mm; radius of fillet, $R = 76$ mm; and thickness, $T = 7$ mm. Four additional specimens were machined to the following geometry for use in strain to failure tests: gage width, $W = 14.6$ mm; length of narrow section, $L = 29$ mm; grip width, WO = 19 mm; overall length, LO = 123 mm; gage length, $G = 25$ mm; distance between grips, $D = 55$ mm; radius of fillet, $R = 38$ mm; and thickness, $T = 7$ mm. A schematic of the specimen geometries is provided in Fig. 1. The specimens were machined such that their long axis was aligned with the extrusion direction. Following machining, half of the mechanical specimens were sterilized in a nitrogen environment using 25 kGy of γ-radiation from a ^{60}Co source (Raychem Corp., Menlo Park, CA). The specimens were then allowed to age in air for four years prior to mechanical testing.

2.2. Mechanical characterization

2.2.1. True stress–strain behavior

Tension tests were conducted using an Instron 5500 (Canton, MA) screw-driven mechanical test system. To evaluate the strain during the tests, a custom video-based strain measurement system was developed and validated to characterize the true stress–strain behavior. Parallel gage marks were drawn in ink orthogonal to the tensile direction at 2.5 mm intervals within the gage region on both cross-sections of the specimens. In addition, parallel gage marks were also drawn at 5.0 mm intervals in line with the tensile direction on the large face of the specimens. A special jig was designed to ensure that the grid lines were drawn parallel and precise. During the tension tests, two stationary Mini-DV digital camcorders (Canon USA, Lake Success, NY) were positioned such that there was one camera orthogonal to each cross-section of the specimen. Further, the cameras were oriented such that the gage region of the specimen occupied the maximum field of view in the camera's CCD (i.e. the camera's CCD consisted of 720 by 480 effective pixels, and the camera was oriented such that the gage region was parallel with the 720 pixel axis). Grid markers were also placed in the field of view of each camera to provide a constant length dimension that could be correlated with later pixel measurements. Efforts were made to maintain the entire gage region within the field of view of the camera while maximizing the number of pixels occupied by the specimen to minimize uncertainty.

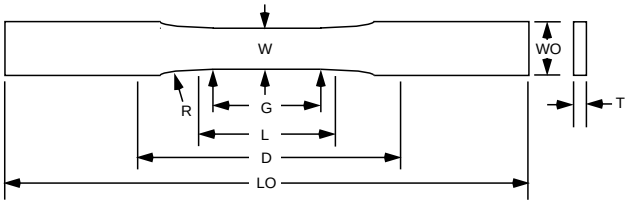

Fig. 1. Schematic illustration of the dog bone specimens used in cyclic strain studies.

A strobe light was utilized to synchronize the cameras to each other and to the computer data recorder attached to the Instron mechanical test system. The computer data was then correlated to the digital time code imprinted on the video to within 1/30 s (1 frame). The digital video pictures were transferred directly to a micro-computer with a Digital Origin 1394 FireWire host adapter card (Mountain View, CA) using the IEEE 1394 standard. The digital pictures were imported into Adobe Photoshop LE (San Jose, CA) where the gage length and specimen width and thickness were measured in pixels. The pixel measurements for the width and thickness were converted to units of length using the grid markers described above to calculate the specimen cross-sectional area. The true stress and homogeneous true strain were calculated using the following equations:

$$\sigma = \frac{P}{A}, \qquad \epsilon = \ln\frac{L}{L_0}$$

where P is the load, A is the current cross-sectional area, L_0 is the pixel-based initial length of the gage region and L is final length of the gage region. The true strain described in the equation above should be identified more correctly as the homogeneous strain since it assumes that the strain is homogeneous throughout the gage length (or length of concern). To determine the true strain at a point, or for inhomogeneous deformation, the strain should be defined as follows:

$$\epsilon = \lim_{l_0 \to 0}\left[\ln\frac{l}{l_0}\right]$$

where l and l_0 are the initial and current lengths of the section of the specimen over which the strain is assumed to be homogeneous. At times during some of the tests, the end points of the gage region left the field of view of the camera. When this occurred, L was defined by the

Table 2
Summary of combinations of number of cycles and true strain utilized for the cyclic tests

Material	Number of cycles	True strain
Non-sterilized	1	0.5, 1.0
	10	0.5, 1.0
	100	0.5, 0.12
Sterilized	1	0.5, 1.0
	10	0.5, 1.0
	100	0.5, 0.12

pixel distance between the two lines with the greatest separation that were still within the field of view of the camera, and L_0 was defined as the pixel distance between these same two lines initially. The error associated with this alternative measurement was significant only in regions of large inhomogeneous strain. Kurtz et al. [2], using a similar video-based strain measurement system, demonstrated that the true strain uncertainties associated with this pixel-based measurement are large for strains less than 5% but decrease significantly at larger strains. Conversely, the true stress uncertainties begin small and increase with increasing strain due to the reduction in the number of pixels representing the width and thickness of the specimen. The relative uncertainty in the true strain was found to increase asymptotically as the strain approached zero and decreased as the strains increased, whereas the relative uncertainty in the true stress increased with increasing strain to a maximum of approximately 0.065.

Prior to conducting the cyclic tension tests, four specimens (two non-sterilized and two sterilized) were strained to the maximum extension to determine the best extension rate and to generate true strain versus extension curves that could be utilized for the follow-on tests. Furthermore, to validate the accuracy of the custom video-based strain measurement system, a preliminary test was conducted to 0.1 strain with a conventional extensometer. Twelve cyclic uniaxial strain tests were conducted (six on the non-sterilized specimens and six on the sterilized specimens) at a constant extension rate of 20 mm/min at room temperature (23 ± 3°C). Table 2 provides the combinations of number of cycles and true strain utilized for the tests. The cycles comprised triangle patterns, and one cycle consisted of stretching the specimen to a specified extension at a constant rate and then contracting the specimen at the same 'extension' rate until zero load. The required extension for the desired true strain was determined using the true strain versus extension curves generated initially. Strain values of 0.50 and 1.00 were chosen to provide sufficient deformation to allow for morphological changes in the UHMWPE. The strain value of 0.12 was chosen since finite element models of tibial components have suggested that the maximum effective (von Mises) strain is approximately 0.12 in orthopedic devices, and it was desired to determine if morphological changes could be seen at these smaller, clinical strains. Cycles of 1, 10, and 100 were chosen to provide an order of magnitude difference between

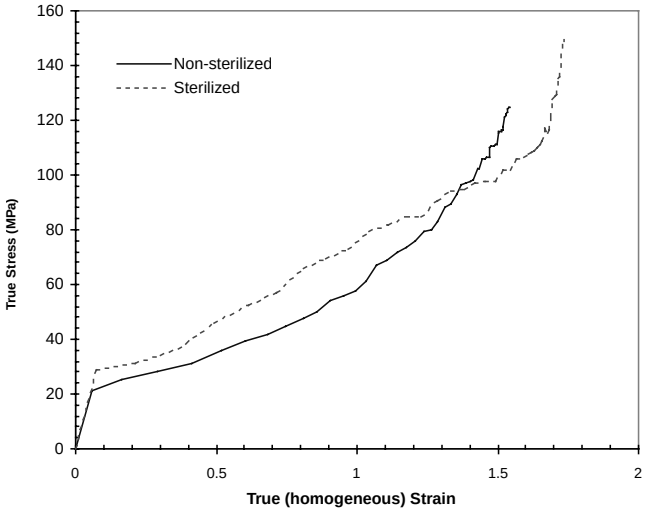

Fig. 2. True stress–strain curves for non-sterilized and sterilized UHMWPE for strain to failure test.

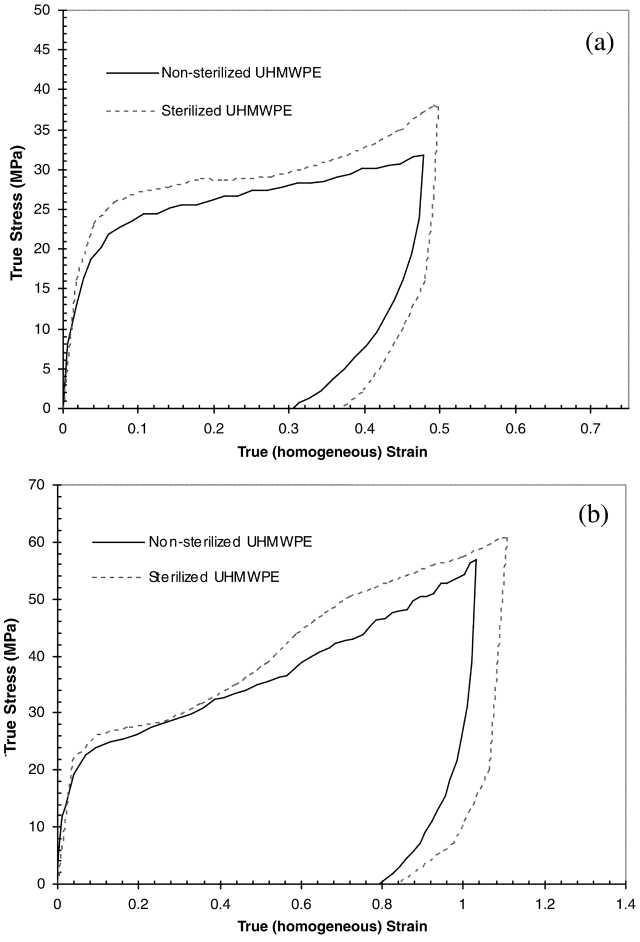

Fig. 3. Single cycle true stress–strain curves for non-sterilized and sterilized UHMWPE: (a) to 0.50 true strain; and (b) to 1.00 true strain.

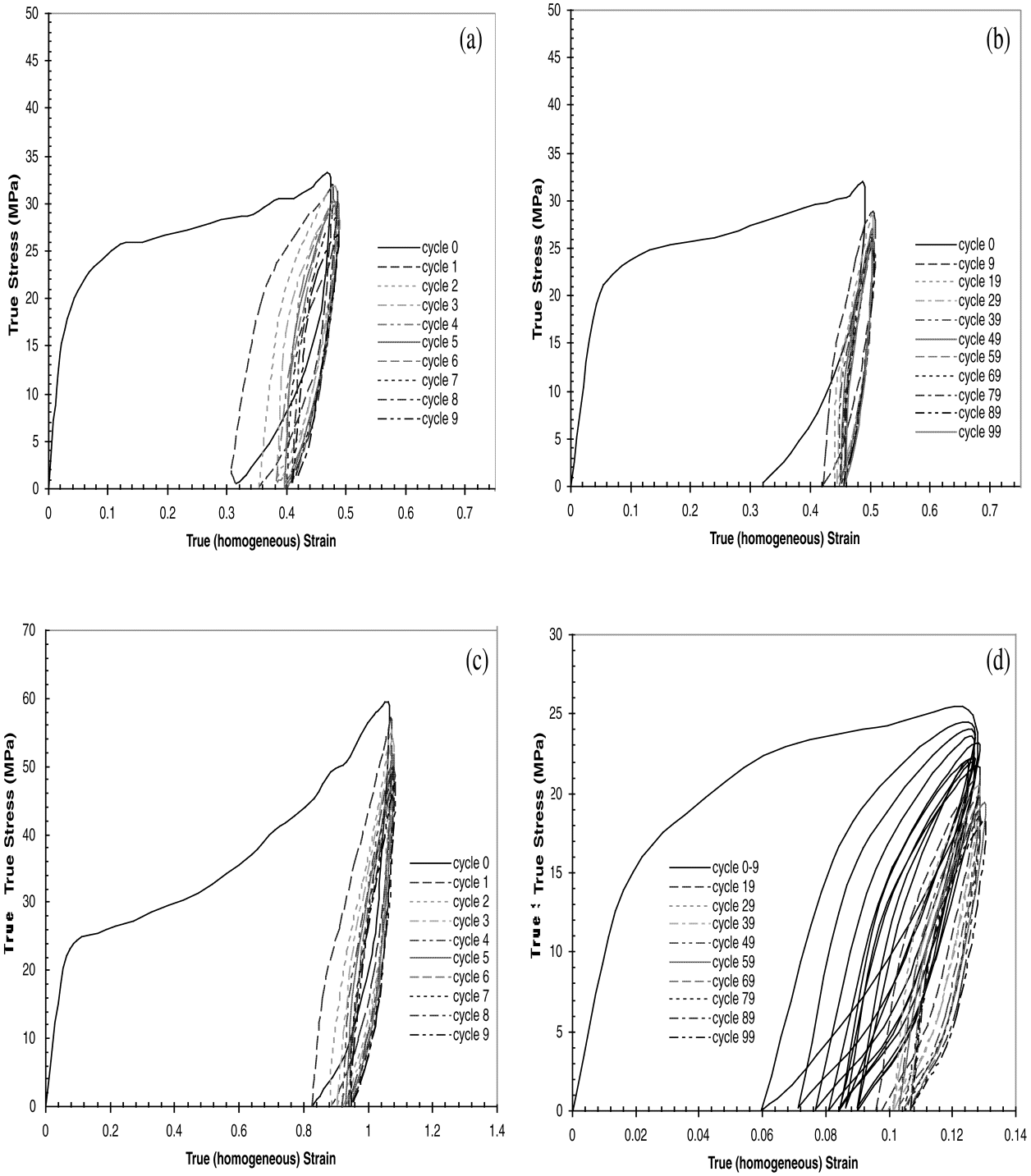

Fig. 4. Cyclic true stress–strain curves for non-sterile UHMWPE: (a) 10 cycles to 0.50 true strain; (b) 100 cycles to 1.00 true strain; (c) 10 cycles to 1.00 true strain; and (d) 100 cycles to 0.12 true strain.

the cycles to help ensure statistical significance of any morphological differences noted.

2.2.2. Strain recovery

Immediately following each cyclic test, the specimens were removed from the Instron grips to determine their viscoelastic recovery behavior. The specimen gage length was measured continuously over a period of days and utilized to determine the specimen's true strain versus time behavior. Measurements were taken until the percent change in the gage length between measurements taken at least five days apart was less than 0.2%. This final strain was

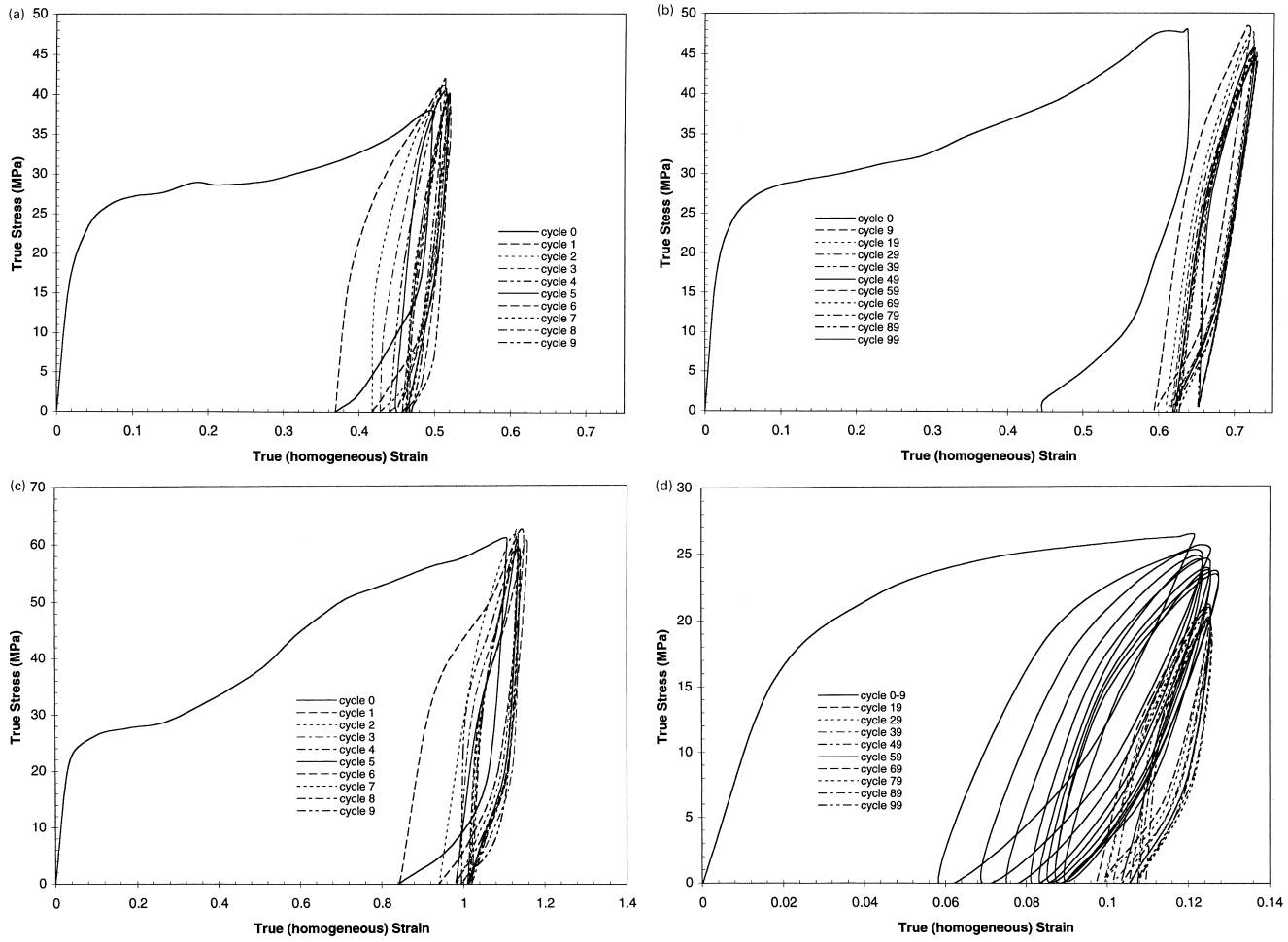

Fig. 5. Cyclic true stress–strain curves for sterilized UHMWPE: (a) 10 cycles to 0.50 true strain; (b) 100 cycles to 1.00 true strain; (c) 10 cycles to 1.00 true strain; and (d) 100 cycles to 0.12 true strain.

identified as the residual long-term plastic strain in the specimens.

2.3. Structural characterization

2.3.1. Density gradient column measurements

After the specimens had completely recovered as defined above, they were sectioned for density characterization using a density gradient column (DGC) of distilled water and isopropanol. The DGC was prepared in accordance with ASTM D1505-85 standard. Three samples from each group, each approximately $5 \times 3 \times 1$ mm^3, were studied. These samples were sectioned from the specimens in the region of maximum localized strain or the center of the gage length if the region of maximum localized strain was not readily identifiable.

2.3.2. Fractography

To confirm the results obtained in the density characterization, the four small dog bones described above were strained to failure. The fractured surfaces of these four specimens and surface cracks that formed during these tests and on earlier specimens were sputter-coated with Au–Pd and examined using a JEOL 35CF scanning electron microscope. Additionally, for the sterilized material group, a propensity for surface crack initiation was noted and these were also examined using SEM.

2.3.3. Field emission microscopy

Reorganization of lamellae microstructure that occurred in the UHMWPE specimens subjected to cyclic strain were analyzed using a LEO 1550 Schottky FEM. Samples were sectioned from the specimens in the same region from which the density specimens were removed so the density changes could be correlated with morphological evolution. In order to study the crystalline lamellae, the samples were etched for 2 h in a sonicator using a permanganic acid etching technique similar to that described by Naylor and Phillips [38] and originally described by Hodge and Bassett [39]. The details of the etching technique used in this study are described

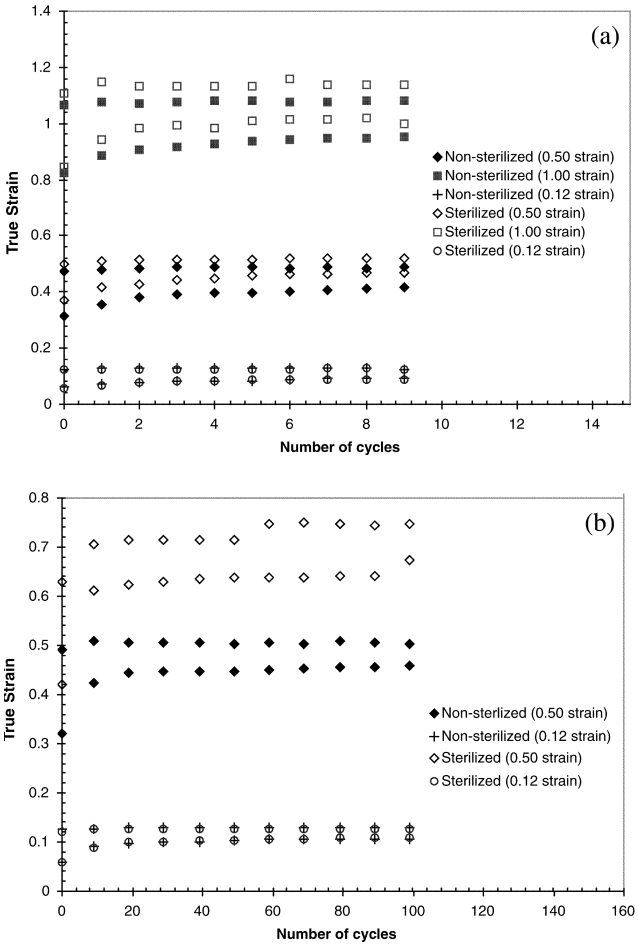

Fig. 6. Maximum and minimum true strain versus number of cycles for non-sterilized and sterilized UHMWPE: (a) 10 cycle tests; and (b) 100 cycle tests.

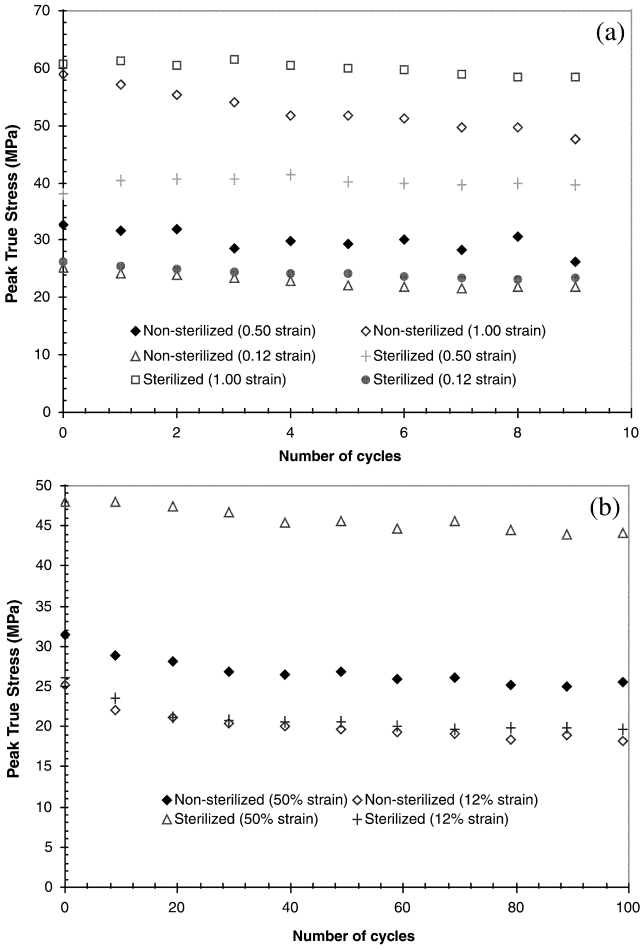

Fig. 7. Maximum peak true stress versus number of cycles for non-sterilized and sterilized UHMWPE: (a) 10 cycle tests; and (b) 100 cycle tests.

elsewhere [40]. Following etching and rinsing, the samples were sputter coated with Au and examined with the FEM.

3. Results and discussion

3.1. True stress–strain behavior

The results of this study clearly indicate that a video-based measurement system is an accurate means of determining the true stress–strain behavior of UHMWPE at large cyclic deformations. During the validation experiment and during the cyclic strain tests to 0.12 true strain, the video-based estimates of true homogeneous strain compared favorably with the extensometer-based estimates. At strains greater than 0.01, the two methods agreed exceptionally well, and the average difference between the two methods throughout the entire strain range was less than 5%. The results from video-based measurement systems are arguably best when the mechanical behavior of the polymer fulfills two criteria: (1) incompressible behavior; and (2) homogeneous deformation in the gage region. By measuring both the cross-sectional area and the elongation of the specimen explicitly, as was done in this study, the need for the incompressible behavior is negated. Homogeneous deformation is satisfied in the absence of localized necking. Non-homogeneous behavior associated with necking can still be characterized with this system but is done with the use of the expression for localized strain.

During the cyclic uniaxial tension tests, the non-sterilized UHMWPE specimens deformed relatively homogeneously, exhibiting little or no macroscopic necking in the gage region. The sterilized specimens, however, typically necked within the gage region, and this neck then propagated along the gage region as the strain increased. This neck in the sterilized specimens resulted in the cyclic load being concentrated in a fairly narrow region of the dog bone, especially for the specimens subjected to lower strains. Both the non-sterilized and sterilized specimens showed evidence of increased opacity or whitening during the tension tests, consistent with cavitation and the nucleation of internal microvoids. The sterilized specimens, though, showed a much greater tendency for stress whitening than

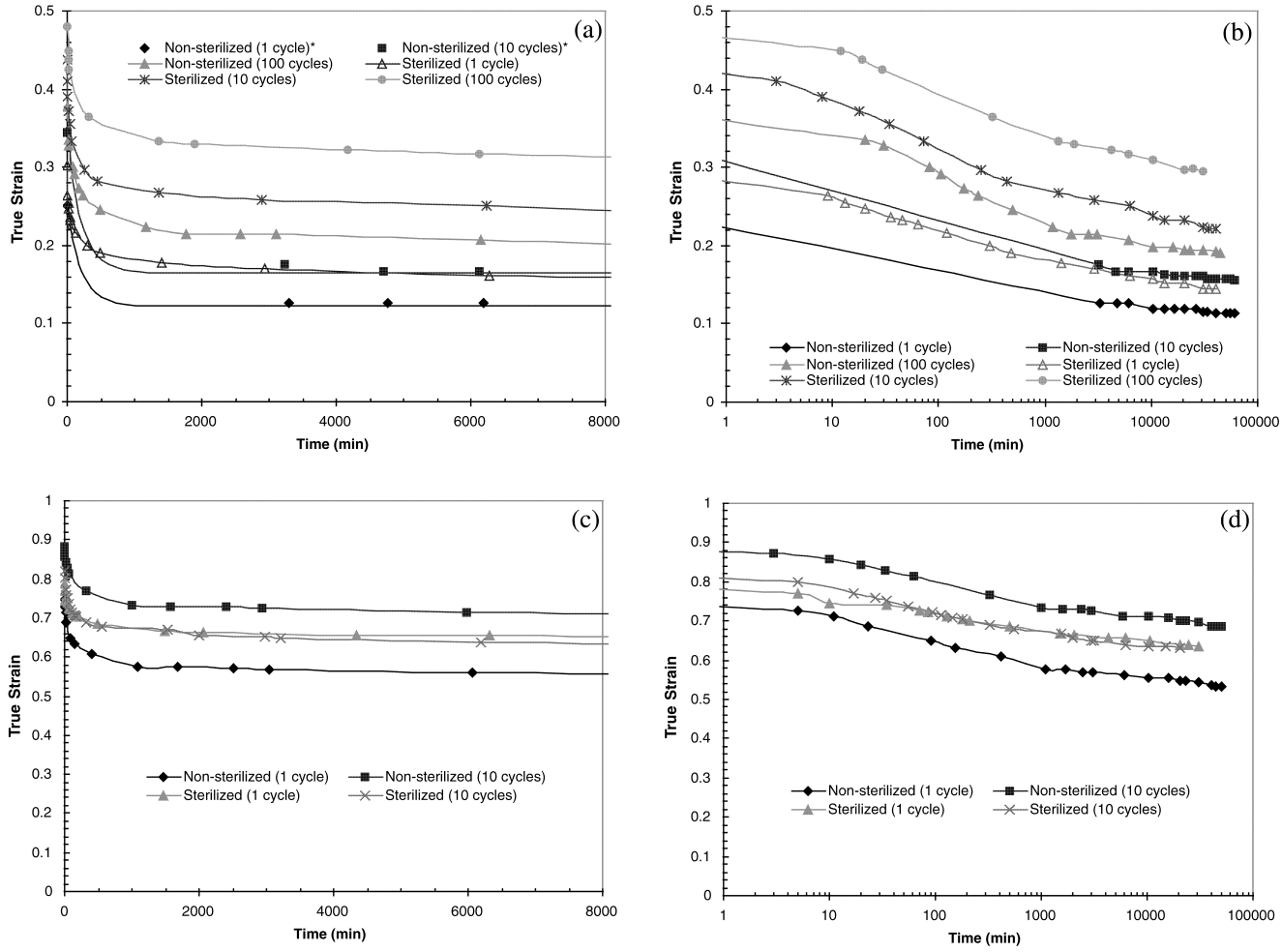

Fig. 8. Strain recovery for non-sterilized and sterilized UHMWPE: (a) cyclic true strain of 0.50; and (b) cyclic true strain of 1.00.

did the non-sterilized specimens. This is likely due to numerous surface crazes and subsequent surface cracks that were found to occur in the sterilized UHMWPE.

Representative true stress–strain curves from the strain to failure tests for the UHMWPE are shown in Fig. 2. Both the non-sterilized and sterilized UHMWPE undergo strain hardening following a fairly well-defined knee in the true stress–strain curves. This knee corresponds to the onset of localized necking in the sterilized specimen. Note that the sterilized UHMWPE exhibits an initially stiffer behavior and a higher yield stress than the non-sterile control. The sterilized material, having been exposed to γ-radiation and aged in air, is known to have a higher degree of chain scission, a higher degree of follow-on oxidation, and greater crystallinity than the non-sterilized material [15–17]. The greater initial density of the sterilized material supports this contention. The higher crystallinity of the sterilized material may assist with the resistance to the initial deformation but the decreased molecular weight owing to chain scission and oxidation lends itself to greater propensity for fibrillation and cavitation mechanisms. This is evidenced by the large decrease in density with cyclic straining and the fractography observed for the sterilized polymer (discussed below).

Figs. 3–5 provide the cyclic true stress–strain behavior for the UHMWPE specimens for a range of true strains and loading cycles. For ease of comparison, the non-sterilized and sterilized UHMWPE cyclic true stress–strain plots are overlaid in Fig. 3 to show the results of a single loading cycle. Figs. 4 and 5 show the cyclic true strain curves for cyclic true strains ranging from 0.12 to 1.0 for both the non-sterile and radiation aged UHMWPE, respectively. These plots reveal that UHMWPE, like most polymers, exhibit an elastic behavior during cyclic loading. This effect is extremely large initially, as demonstrated by the large initial hysteresis loops, and it diminishes with increasing number of cycles. Although the hysteresis loops shrink with increasing number of cycles, they do not completely disappear.

Fig. 6 shows the change in the maximum and minimum true strain achieved per cycle for the (a) 10 and (b) 100 cycle tests. While the maximum and minimum true strain increase with every cycle, the rate of increase decreases as the

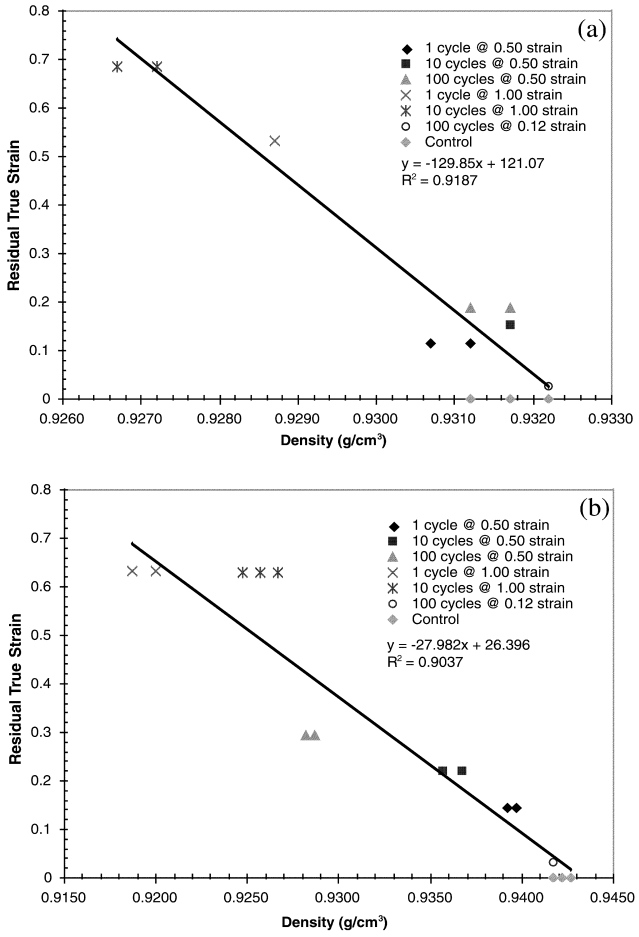

Fig. 9. Density of (a) non-sterile, and (b) sterilized UHMWPE as a function of plastic strain.

number of cycles increases. The rate of change does not completely diminish nor do the hysteresis loops completely saturate within 100 cycles. However, based on the trends exhibited by both the non-sterilized and sterilized UHMWPE, it is likely, that with a greater numbers of cycles, saturation would be reached. The maximum true stress of the UHMWPE also changes cyclic loading. As shown by Fig. 7, the non-sterilized UHMWPE undergoes cyclic strain softening as the peak true stress achieved during any cycle drops with increasing number of cycles. The sterilized UHMWPE initially undergoes cyclic strain hardening for about the first five cycles, followed by cyclic strain softening similar to the non-sterilized material. Similarly to the true strain behavior versus the number of cycles, the cyclic softening rate decreases with increasing number of cycles, and it does not saturate within 100 cycles. The cyclic strain softening suggest that cyclic damage accumulates in the polymer with continued loading resulting in changes to recoverability and morphology of the polymer as discussed below.

3.2. Strain recovery

This cyclic damage described above strongly affects the strain recovery and residual plasticity of the UHMWPE. The UHMWPE exhibits highly non-linear strain recovery behavior, where the majority of the recovery occurred within one day after removing the load. Fig. 8 shows the true strain recovery behavior for both the non-sterilized and sterilized UHMWPE for cyclic true strain conditions of (a) 0.5 and (b) 1.0. It is clear from the plots of strain recovery that the cyclic loading of the UHMWPE affects its residual plasticity where the greater the number of cycles results in greater levels of residual plasticity. This effect is found to be greater for the sterilized material than the non-sterilized material at lower strains and is further enhanced in the non-sterile material at higher strains. If the data are normalized by the maximum true strain applied during each individual test, then it becomes apparent that the amount of true strain applied has a greater effect on residual plasticity than does the number of cycles. As expected, the larger degree of true strain applied results in greater levels of residual plasticity.

3.3. Density gradient column measurements

The densities for the non-sterilized and sterilized UHMWPE as a function of residual true strain are given in Fig. 9. This figure shows that the density decreases linearly with increasing residual true strain for both the non-sterilized ($r^2 = 0.9187$) and the radiation sterilized ($r^2 = 0.9037$) UHMWPE. The linear relationship between density and residual true strain provides remarkable evidence of a morphological evolution in UHMWPE directly related to the cyclic strain behavior. The results show that the residual plasticity in both the non-sterilized and the sterilized UHMWPE is a function of both the amount of true strain and the number of cycles applied to the specimens. Furthermore, as indicated by the linear decrease in density with increasing residual true strain, the density in UHMWPE is directly related to the residual true strain (while still also a function of other factors, such as crystallinity, molecular weight, degree of oxidation, etc.). While density depends on many factors, the density decrease in the UHMWPE due to cyclic loading is most likely attributed to microvoid formation and fibrillation. Such damage is associated with micromechanisms such as crazing in the polymer [37]. It is believed that the cavitation of the amorphous regions occurs preferentially if this phase is weakened due to low molecular weight or low degree of interlamellar connectedness associated with chain scission and oxidation. Thus, a greater susceptibility to crazing mechanisms is postulated to occur in the sterilized material due to enhanced pathways of cavitation in the polymer [41,42]. This is supported by the

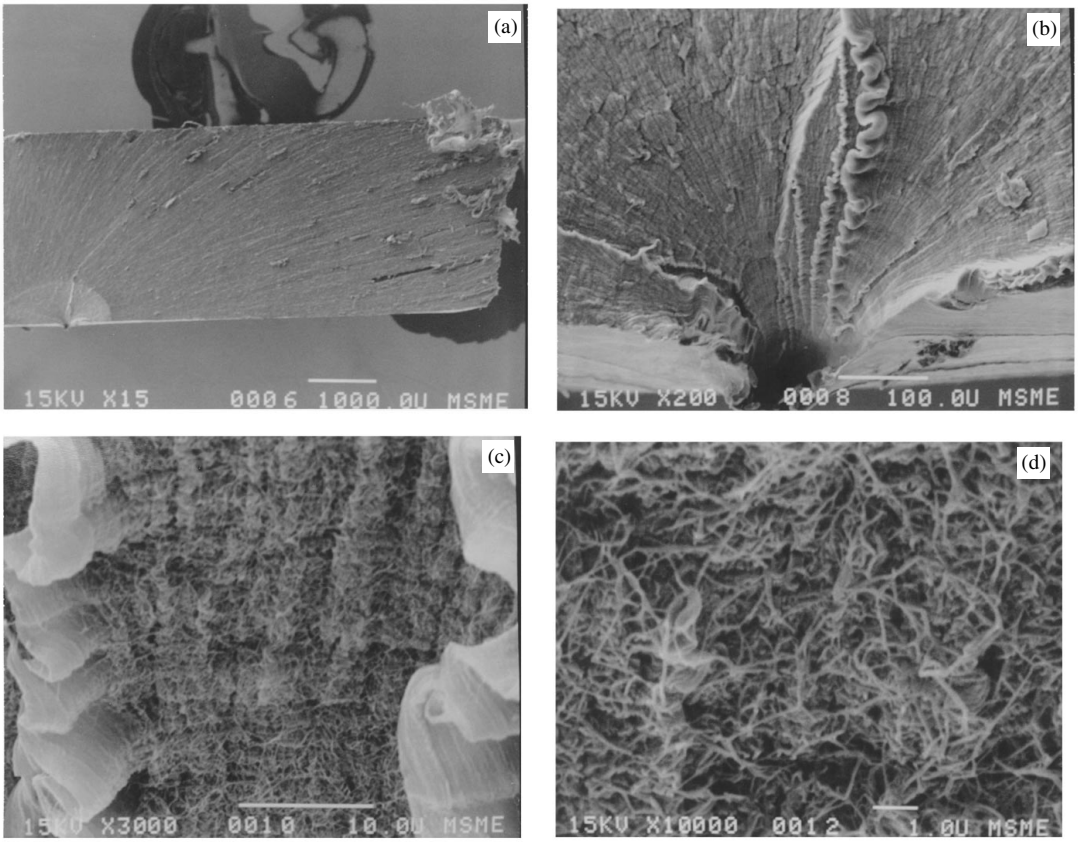

Fig. 10. Scanning electron micrographs of non-sterilized UHMWPE. (a) Planar fracture surface showing ductile and brittle behavior (15×). (b) Failure initiation defect at 200× magnification. (c) Craze region at high magnification (3000×), showing circumferential ridges and fibrils. (d) Craze region at high magnification (10,000×), showing circumferential ridges and fibrils.

observed density decrease that is enhanced for the sterilized UHMWPE.

3.4. Fractography

Fractography using SEM of the UHMWPE indicate that microvoid formation followed by fibrillation and crazing is the micromechanistic pathway for cyclic damage. This behavior was more prominent in the aged, sterilized polymer. Representative scanning electron micrographs showing the fracture surfaces of the non-sterilized and sterilized UHMWPE are given in Figs. 10 and 11. In the non-sterilized UHMWPE the fracture appeared to initiate at a defect (Fig. 10a). Around this defect the fracture surface displayed concentric, circumferential features characteristic of the nucleation and slow crack growth mechanisms of void coalescence and fibrillation. These

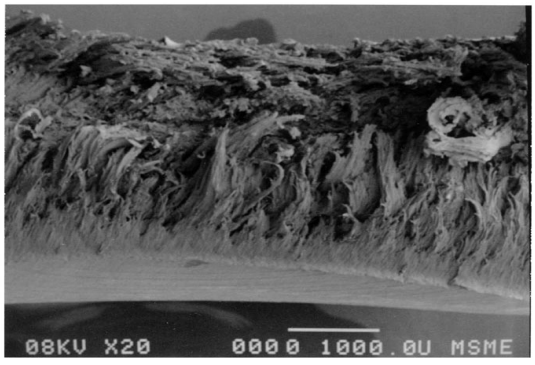

Fig. 11. Scanning electron micrographs of sterilized UHMWPE fracture surface showing fibrillation.

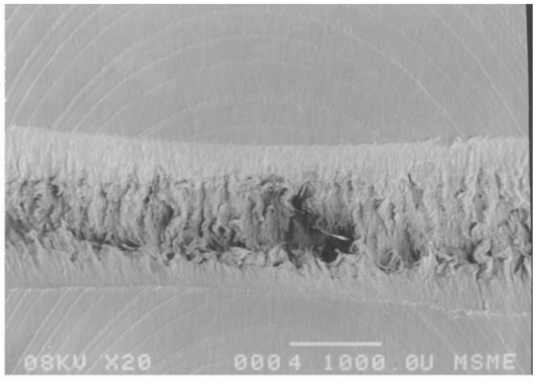

Fig. 12. Scanning electron micrograph of a typical surface crack observed in the sterilized UHMWPE.

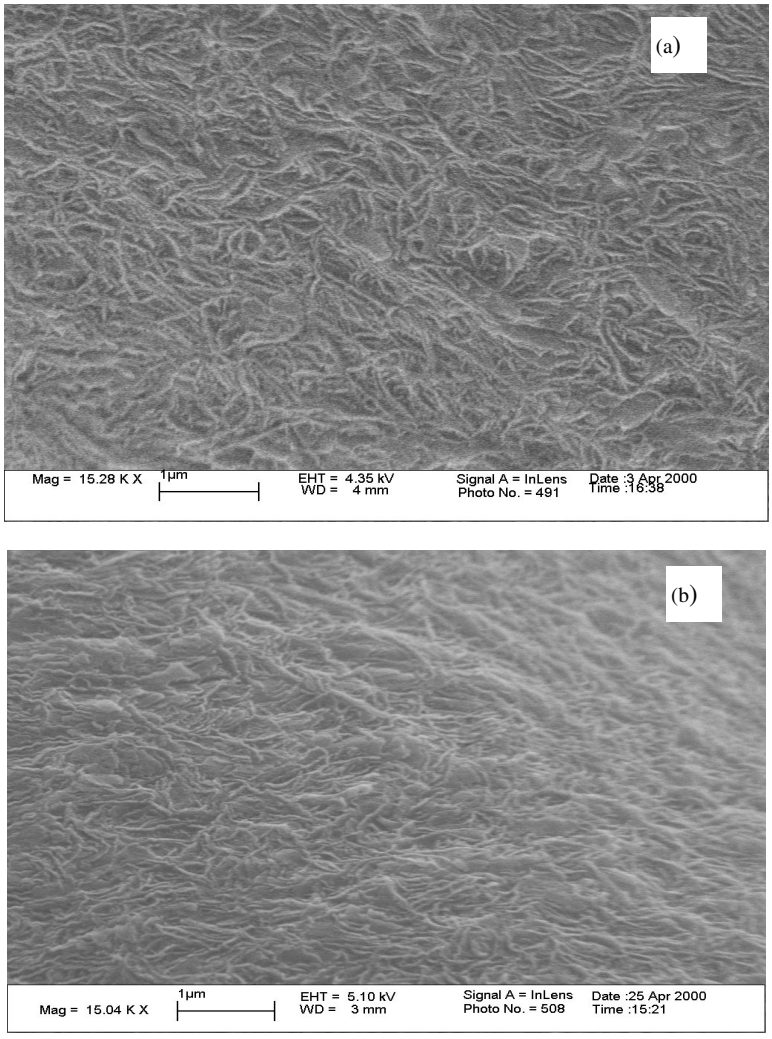

Fig. 13. Field emission micrographs of non-sterilized UHMWPE specimens: (a) unstrained; (b) one cycle to 0.50 true strain; (c) 100 cycles to 0.50 true strain; (d) one cycle to 1.00 true strain; (e) 10 cycles to 1.00 true strain; and (f) 100 cycles to 0.12 true strain.

micromechanisms are indicative of crazing at the defect site. The fracture surface of the sterilized UHMWPE (Fig. 11) shows large, macroscopic fibrils, characteristic of localized plasticity and extreme fibrillation of the polyethylene. These large fibrils are also evident in the surface cracks that formed on the sterilized specimens (Fig. 12). These fibrils suggest significant cavitation and void formation within the sterilized UHMWPE during plastic deformation.

Since the irradiated UHMWPE is more crystalline than the non-sterile material, the former will exhaust the amorphous component of deformation more quickly than the non-sterilized material, and it will experience more residual plasticity at lower strains. Thus, at low strains cyclic plastic damage is expected to be more prominent in the sterilized material than the non-sterilized material. The results of this study support this: at low strains the sterilized material exhibits greater residual true strain following cyclic loading than does the non-sterilized material. Furthermore, as lamellae alignment is related to residual plasticity, the FEM (described below) also supports this contention.

3.5. Field emission microscopy

Field emission micrographs of the UHMWPE specimens are provided in Fig. 13a–f. All figures are oriented such that the tensile direction is along the horizontal axis. Fig. 13a is a micrograph of unstrained non-sterilized UHMWPE (the non-sterilized control). The lamellae are clearly visible, and it is apparent from the figure that the lamellae in the unstrained polymer are randomly oriented (i.e. the extrusion process did not have a noticeable effect on the lamellae morphology). The non-sterilized specimens subjected to one cycle and 100 cycles at 0.50 true strain are shown in Fig. 13b and c, respectively. The lamellae in these specimens show only a small degree of alignment; however, the specimen subjected to 100 cycles does exhibit a slightly greater degree of alignment than the specimen subjected

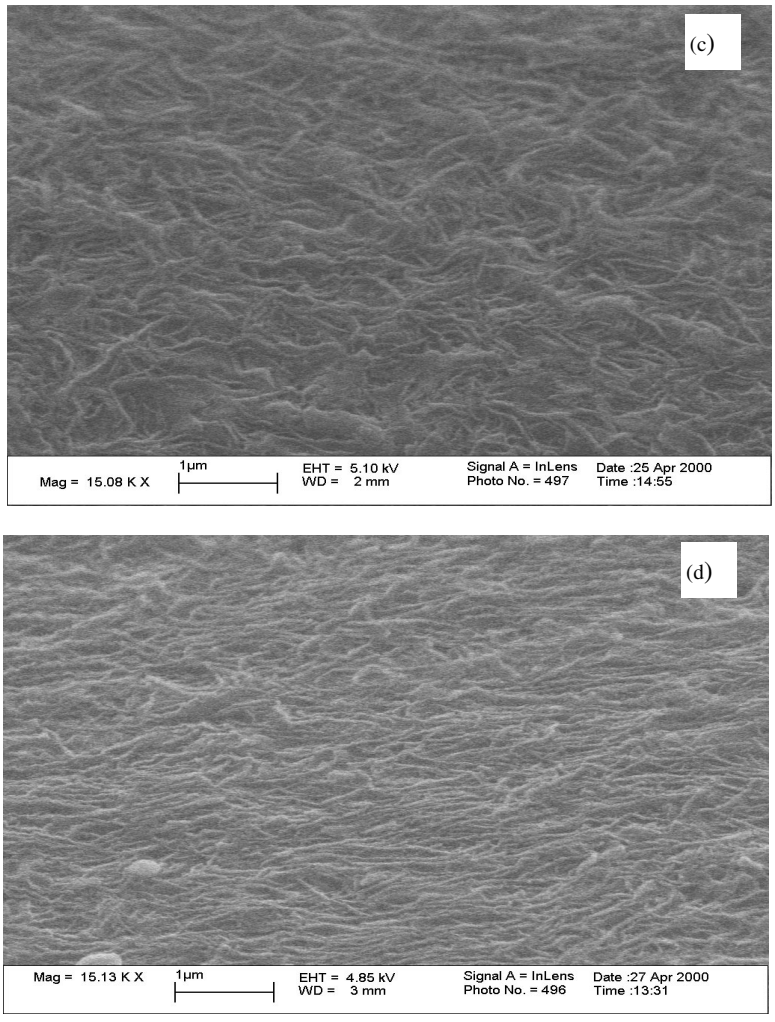

Fig. 13. (*continued*)

to only one cycle. In contrast to the specimens subjected to 0.50 true strain, those subjected to 1.00 true strain show considerable texturing (Fig. 13d and e). The lamellae in these specimens are highly aligned with the tensile direction. However, no appreciable difference can be ascertained between the specimen that was cycled 10 times and the specimen that was cycled only one time. Finally, the lamellae in the specimen subjected to 100 cycles at 0.12 true strain appear to remain randomly oriented and show no significant alignment (Fig. 13f). The sterilized UHMWPE shows a similar progression of texture evolution with increasing strain and loading cycles. The FEM provides the greatest direct evidence of the morphological evolution of the UHMWPE as a function of the amount of true strain and the number of cycles. It was found from the FEM study that with increasing strain for both the non-sterilized and sterilized UHMWPE there is an increasing degree of lamellae alignment. Furthermore, increased lamellae alignment is also observed with increasing number of cycles, and this effect is much more prevalent in the sterilized material than the non-sterilized material at low strains. The cyclic nature of the strain most likely helps to initiate a greater number of slip systems, resulting in greater alignment for a greater number of cycles. At higher strains both materials activate crystalline slip systems, and thus both materials exhibit substantial amounts of lamellae alignment. This finding is important as texture development in UHMWPE has been linked with wear mechanisms in total joint replacements.

4. Conclusions

This study utilized a video-based measurement system as an accurate means of determining the true stress–strain behavior of UHMWPE at large cyclic deformations. This work characterized the cyclic true stress–strain behavior of both non-sterilized and sterilized GUR 4150 UHMWPE. The results indicated that the mechanical behavior of the materials could be attributed to their microstructural differences, and with the use of SEM and FEM showed that the polymer mechanical properties could be correlated

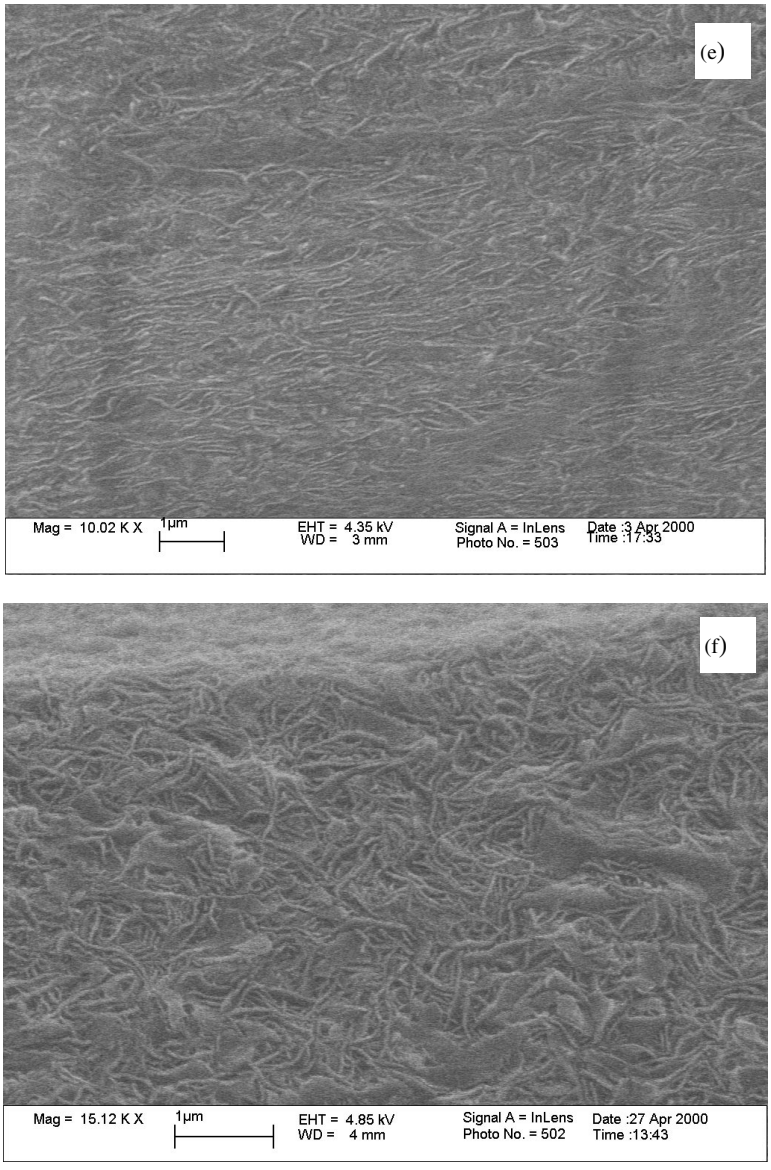

Fig. 13. (*continued*)

with the morphological evolution of the UHMWPE during the cyclic tests. Residual plastic strain was found to increase with increasing amount of true strain and number of cycles, and density was found to decrease linearly with increasing residual plastic strain. Crazing and microvoid formation influenced both of these results. Moreover, lamellae alignment was also found to increase with increasing amount of true strain and number of cycles. The degree of texture development differed between the non-sterilized and sterilized UHMWPE, and this contrast was attributed to the initial microstructure of each material. This study clearly shows that γ-radiation and subsequent aging has an embrittling effect on the UHMWPE resulting in microvoid and crazing mechanisms that can lead to premature fracture in total joint prostheses. The findings from this study have important implications for the development of future constitutive models that incorporate the microstructural evolution in polymers subjected to cyclic loading conditions.

Acknowledgements

This research was funded by the Office of Naval Research under Grant No. N00014-98-1-0633 and the National Science Foundation under Grant No. CMS-9624978 to the University of California, Berkeley. The authors would like to thank Ms Christina Hwang for conducting the field emission microscopy and Mr Wesley Jackson, Ms Meera Sankara, and Ms Ruhi Kumar for their assistance in capturing video images of the strain tests.

References

[1] Li S, Burstein AH. J Bone Jt Surg 1994;76-A:1080.
[2] Kurtz SM, Pruitt L, Jewet CW, Crawford RP, Crane DJ, Edidin AA. Biomaterials 1998;19:1989.
[3] Wang A, Stark C, Dumbleton JH. J Biomed Mater Res 1995;29:619.
[4] G'Sell C, Jonas JJ. J Mater Sci 1979;14:583.
[5] Baker DA, Hastings RS, Pruitt L. J Biomed Mater Res 1999;46:573.
[6] Bartel DL, Rawlinson JJ, Burstein AH, Ranawat CS, Flynn WF. Clin Orthop Relat Res 1986;317:76.
[7] Pruitt L, Bailey L. Polymer 1998;39:1545.
[8] Baker DA, Hastings RS, Pruitt L. Polymer 2000;40:795.
[9] Edidin AA, Pruitt L, Jewett CW, Crane DJ, Roberts D. J Arthroplasty 1999;14:616.
[10] Kurtz SM, Pruitt L, Jewett C, Foulds JR, Edidin AA. Biomaterials 1999;20:1449.
[11] Wang HC, Sung C, Hamilton J. J Mater Sci Lett 1998;17:41.
[12] G'Sell C, Dahoun A. Mater Sci Engng, A 1994;175:183.
[13] Dole M. Radiation chemistry of macromolecules. New York: Academic Press, 1972.
[14] Goldman M, Gronsky R, Ranganathan R, Pruitt L. Polymer 1996;37:2909.
[15] Shinde A, Salovey RJ. J Polym Sci Lett 1985;23:1681.
[16] Goldman M. PhD dissertation, University of California, Berkeley, 1997.
[17] Goldman M, Lee M, Gronsky R, Pruitt L. J Biomater Res 1997;37:43.
[18] Goldman M, Gronsky R, Long GG, Pruitt L. Polym Degrad Stab 1998;62:97.
[19] Katagiri T, Sugimoto M, Nakanishi E, Hibi S. Polymer 1993;34:487.
[20] Peterlin A. J Mater Sci 1971;6:490.
[21] Galeski A, Bartezak Z, Argon AS, Cohen RE. Macromolecules 1992;25:5705.
[22] Lin L, Argon AS. J Mater Sci 1994;29:294.
[23] G'Sell C, Hiver JM, Dahoun A, Souahi A. J Mater Sci 1992;27:5031.
[24] Wimmer M. J Arthroplasty 1998;13:8.
[25] Young R, Bowden PB. Philos Mag 1974;29:1061.
[26] Young RJ, Bowden PB, Ritchie JM, Rider JG. J Mater Sci 1973;8:23.
[27] Hay IL, Keller A. Kolloid Z. Z. Polym 1965;204:43.
[28] Pope DP, Keller A. J Polym Sci, Polym Phys Ed 1975;13:533.
[29] Groves GW, Hirsch PB. J Mater Sci 1969;4:929.
[30] Tagawa T. J Polym Sci, Polym Phys Ed 1980;18:971.
[31] Frank FC, Keller A, O'Connor A. Philos Mag 1958;3:64.
[32] Bevis M, Crocker AG. Proc R Soc 1965;288:240.
[33] Wu W, Argon AS, Turner APL. J Polym Sci, Polym Phys Ed 1972;10:2379.
[34] Meinel G, Peterlin A. J Polym Sci 1971;9:67–83.
[35] Kitagawa M, Onoda T, Mizutani K. J Mater Sci 1992;27:13–23.
[36] Kitagawa M, Qui J, Nishida K, Yoneyama T. J Mater Sci 1992;27:1449–56.
[37] Kausch HH, Gensler R, Grein CH, Plummer CJG, Scaramuzzino P. J Macromol Sci, Phys B 1999;38:803–15.
[38] Naylor KL, Phillips PJ. J Polym Sci 1983;21:2011–26.
[39] Hodge AM, Basset DC. J Mater Sci 1977;12:2065.
[40] Meyer R. MS thesis, University of California, Berkeley, 2000.
[41] Zeng ZP, Buggy M, Griffin J, Little EG. J Mater Sci: Mater Med 1992;3:255–61.
[42] Duan DM, Williams JG. J Mater Sci 1998;33:625–38.